



Characterization of spatial distribution of tumor-infiltrating CD8⁺ T cells refines their prognostic utility for pancreatic cancer survival

Yohei Masugi¹ · Tokiya Abe¹ · Akihisa Ueno¹ · Yoko Fujii-Nishimura¹ · Hidenori Ojima¹ · Yutaka Endo^{1,2} · Yusuke Fujita² · Minoru Kitago² · Masahiro Shinoda² · Yuko Kitagawa² · Michiie Sakamoto¹

Received: 28 January 2019 / Revised: 30 April 2019 / Accepted: 1 May 2019 / Published online: 11 June 2019
© United States & Canadian Academy of Pathology 2019

Abstract

The abundance of cytotoxic T-cell infiltrates has important implications for patient outcome and therapeutic design for pancreatic ductal adenocarcinoma. However, intratumoral heterogeneity remains a challenge to understanding the complex immune microenvironment. We hypothesized that characterizing CD8⁺ cell distribution within pancreatic adenocarcinoma tissues might refine the prognostic value of tumor-infiltrating CD8⁺ lymphocytes. Using multiplex immunohistochemistry-based image analysis on whole-tissue sections of 214 pancreatic ductal adenocarcinomas, we measured CD8⁺ cell densities in the tumor center, the tumor margin, and the whole tumor, along with the proximity of CD8⁺ cells to carcinoma cells. Multivariable Cox regression analysis was performed to assess the associations of CD8⁺ cell densities with pancreatic cancer-specific survival, adjusting for clinicopathologic and immune-related features, including tumor expressions of TP53, SMAD4, and the programmed cell death 1 ligand 1 (CD274, PD-L1) and the extent of tertiary lymphoid structures. There was substantial heterogeneity in CD8⁺ cell density, with the mean density in the tumor center less than half that in the tumor margin. Tumor CD274 expression and extensive tertiary lymphoid structures were appeared to be associated with higher CD8⁺ cell density in the tumor margin ($P = 0.037$ and $P = 0.005$, respectively), but not with that in the tumor center ($P > 0.50$). The association of higher CD8⁺ cell density with prolonged survival was significant for the whole tumor ($P_{\text{trend}} = 0.009$); however, the association was stronger for the tumor center ($P_{\text{trend}} = 0.002$) and insignificant for the tumor margin ($P_{\text{trend}} = 0.07$). Tumor cell–CD8⁺ cell distance correlated strongly with CD8⁺ cell density, whereas the density of CD8⁺ cells proximate to cancer cells exhibited no prognostic association. In conclusion, spatial computational analysis on pancreatic ductal adenocarcinoma reveals the prognostic validity of CD8⁺ cell density in the tumor center, where CD8⁺ cell infiltration is ununiformly restricted, likely suggesting pro-tumorigenic roles of the immunosuppressive tumor microenvironment of pancreatic cancer.

Introduction

Cytotoxic T lymphocytes play a central role in eliminating tumor cells that expose tumor-specific antigens in various

malignancies, including pancreatic ductal adenocarcinoma [1, 2]. Higher CD8⁺ T-cell density in tumor tissues correlates with expressions of cytotoxicity genes and is generally associated with prolonged pancreatic cancer survival [3, 4]. Previous studies have underscored the importance of tertiary lymphoid structures (which constitute a peritumoral lymphoid reaction/response) in T cell priming to enhance local adaptive immunity against pancreatic ductal adenocarcinoma [5–7]. Evidence also indicates that pancreatic cancer patients with abundant cytotoxic T cell infiltration exhibit a better response to chemotherapies [8]. Accumulating translational evidence suggests that agents targeting immunosuppressive microenvironmental factors, including desmoplastic stroma, hyaluronan, macrophages, regulatory T cells, and myeloid cells, likely lead to the increase of local CD8⁺ cell infiltrates, and thereby synergize immune

Supplementary information The online version of this article (<https://doi.org/10.1038/s41379-019-0291-z>) contains supplementary material, which is available to authorized users.

✉ Michiie Sakamoto
msakamot@z5.keio.jp

¹ Department of Pathology, Keio University School of Medicine, Tokyo, Japan

² Department of Surgery, Keio University School of Medicine, Tokyo, Japan

checkpoint blockade, although the single use of checkpoint antibodies has nearly universally failed in the treatment of pancreatic cancer [9–11]. Consequently, the assessment of tumor-infiltrating CD8⁺ cells in pancreatic ductal adenocarcinoma tissues may have clinical implications not only for patient prognosis but also for the development of therapeutic strategies against this deadly disease.

Pancreatic carcinogenesis involves sequential accumulations of genetic and epigenetic alterations under the influence of the host immune response, and thus the tumor immune microenvironment of human pancreatic cancer is functionally and spatially heterogeneous [12–20]. A recent computational study using tissue microarray has attested to the prognostic importance of the spatial distribution of CD8⁺ cells within the tumor microenvironment of pancreatic ductal adenocarcinoma [21]. For colorectal cancer, the Immunoscore, which is generated by combining T cell data from the tumor center and the invasive margin, has emerged as a powerful biomarker for the estimation of survival risk [22]. Work is ongoing to validate the combination of the Immunoscore with the TNM stage to produce a TNM-Immune classification of cancer that goes beyond the TNM staging system [23]. Therefore, we hypothesized that an accurate enumeration of tumor-infiltrating CD8⁺ cells together with their spatial distribution might refine the prognostic utility of cytotoxic T cell infiltrates in patients with pancreatic ductal adenocarcinoma. Because it is challenging to date to replicate the complexity of human immune systems with *in vitro* or *in vivo* experiments, patient tissue-based studies are valuable to better understand the role of immune cells in the tumor microenvironment [24, 25]. To test our hypothesis, we analyzed whole-tissue sections of 214 surgically resected pancreatic cancer specimens utilizing multiplex immunohistochemistry-based image analysis. This approach allowed us to rigorously characterize the distribution pattern of tumor-infiltrating CD8⁺ cells in pancreatic carcinoma tissues. The contribution to the prediction of patient prognosis of tumor-infiltrating CD8⁺ cell density and distribution was examined controlling for tumor and immune-related factors, including tumor expressions of TP53, SMAD4, and the programmed cell death 1 ligand 1 (CD274 or PD-L1), and the extent of tertiary lymphoid structures.

Materials and methods

Study populations and histologic features

We selected 270 consecutive pancreatic ductal adenocarcinoma patients who had undergone pancreatectomy at Keio University Hospital (Tokyo, Japan) between 1991 and 2015. Forty-three of these patients had received

preoperative chemotherapy and/or radiotherapy and were excluded. A further 11 patients with ductal adenocarcinoma variants and mixed tumors, including undifferentiated carcinoma, adenosquamous carcinoma, colloid carcinoma, and mixed ductal-neuroendocrine carcinoma, were also excluded. We did not include two patients for whom we were unable to obtain reliable fluorescent images of tumor tissue because of poor immunohistochemistry-quality. Consequently, we analyzed 214 pancreatic ductal adenocarcinomas with available CD8⁺ cell data for histopathologic study. For four patients who had synchronous and/or metachronous pancreatic ductal adenocarcinomas of multifocal origins, we included only the initially examined main tumors in this study. Tumor differentiation was graded according to the tumor grading system of the World Health Organization (well differentiated – grade 1, moderately differentiated – grade 2, and poorly differentiated – grade 3) [26]. The extent of tertiary lymphoid structures was classified, according to the circumference of peritumoral tertiary lymphoid tissues, as absent, minimal (<50% of circumference), or extensive (≥50%) according to previously described criteria [5] with minor modification. Residual tumor status; stroma type; and the degree of lymphatic invasion, venous invasion, and neural invasion, were recorded according to the Classification of Pancreatic Carcinoma by the Japan Pancreas Society [27]. The tumor stage was defined using the eighth edition of the TNM staging system published by the Union for International Cancer Control (UICC) [28]. The aforementioned histopathologic data were recorded under the approval of at least two pathologists. A centralized pathology review was done by a pancreas-specialized pathologist (Y.M.) blinded to the clinical data. Analyses of human tissue samples were approved by the human subjects committee of the Keio University School of Medicine.

Immunohistochemical analysis

Multiplex fluorescent immunohistochemistry was performed using an automated Bond-Max stainer (Leica Biosystems) with a customized staining protocol based on a poly-horseradish peroxidase-conjugated secondary antibody system combined with tyramide signal amplification. Formalin-fixed, paraffin-embedded sections were dewaxed, rehydrated, and peroxide blocked. Antigen retrieval was carried out by 20 min of heating in Tris-EDTA ER2 solution (Leica Biosystems; catalog number AR9640), followed by blocking with 2.5% normal horse serum and 60 min of incubation with anti-CD8 mouse monoclonal antibody (clone, C8/144B; dilution, 1:200; Nichirei Bioscience; catalog number 413201), 15 min of treatment with anti-mouse ImmPRESS (Vector Laboratories; catalog number MP7402), and 10 min of incubation

with Alexa Fluor 488 Tyramide reagent (Thermo Fisher Scientific; catalog number B40953), according to the manufacturer's instructions. Slides were then reheated for antigen retrieval in ER2 solution (Leica Biosystems), followed by 60 min of incubation with anti-KRT7 (keratin 7) mouse monoclonal antibody (clone, OV-TL 12/30; dilution, 1:200; Agilent; catalog number M701801-2), 15 min of secondary antibody treatment with ImmPRESS, 10 min of incubation with Alexa Fluor 594 Tyramide reagent (Thermo Fisher Scientific; catalog number B40975), and counterstained with Hoechst 33342 (Thermo Fisher Scientific; catalog number H3570). Slides were scanned to obtain three-colored, whole-slide images using a NanoZoomer-XR scanner (Hamamatsu Photonics K.K.; catalog number C12000-03) with a 40× objective lens (Fig. 1a). The slides were further stained with hematoxylin and eosin (H&E) and then rescanned to obtain merged images of H&E images on top of the pre-scanned three-colored images.

Chromogenic immunostaining was performed using monoclonal antibodies: clone DO7 (mouse; dilution, 1:2000; Agilent; catalog number M700101-2) for TP53, clone B-8 (mouse; dilution, 1:100; Santa Cruz Technologies; catalog number sc-7966) for SMAD4, clone E1L3N (rabbit; dilution, 1:100; Cell Signaling Technology; catalog number 13684 S) for CD274 (PD-L1), clone D7U8C (rabbit; dilution, 1:100; Cell Signaling Technology; catalog number 82723) for PDCD1LG2 (PD-L2), clone A3A12 (mouse; dilution, 1:400; Abcam; catalog number ab2785) for LGALS3 (Glectin 3; a ligand for LAG3), clone D9R4A (rabbit; dilution, 1:400; Cell Signaling Technology; catalog number 54330) for LGALS9 [Glectin 9; a ligand for HAVCR (TIM3)], clone 1A4 (mouse; dilution, 1:400; Agilent; catalog number M085101) for ACTA2 (α SMA), clone 236 A/E7 (mouse; dilution, 1:100; Abcam; catalog number ab20034) for FOXP3, clone 10D6 (mouse; dilution, 1:100; Leica Biosystems; catalog number NCL-L-CD163) for CD163, and clone SP330 (rabbit; dilution, 1:100; Abcam; catalog number ab224805) for ITGAM (CD11b). Immunohistochemical analyses for TP53, SMAD4, LGALS3, LGALS9, ACTA2, FOXP3, CD163, and ITGAM were conducted using an automated staining system (Bond Max, Leica Biosystems) with the use of the Bond Polymer Refine Detection Kit (Leica Biosystems). For CD274 and PDCD1LG2 immunohistochemistry, deparaffinized slides were autoclaved in 1-mM Tris-EDTA buffer (pH 9) for antigen retrieval, followed by the primary antibody incubation and the secondary antibody treatment with ImmPRESS (Vector Laboratories; catalog number MP7401). We used human tonsil tissue as the positive control and confirmed strong membrane expression of CD274 in tonsil epithelial cells, and PDCD1LG2 expression in immune cells within germinal centers (Supplementary Fig. 1). Sections processed with these primary

antibodies replaced by phosphate-buffered saline were used as negative controls.

Tumor CD274 expression was interpreted by the study pathologist (Y.M.), who was unaware of other data, to categorize tumors into binary groups based on the percentage of tumor cells expressing CD274 on their membranes, with a threshold of 1%, following the previously published criteria [29]. A second pathologist (A.U.) independently evaluated CD274 immunostaining, and there was excellent concordance between the two observers (kappa value, 0.94). Tumor expressions of TP53 and SMAD4 were evaluated, as previously described [30, 31].

CD8⁺ cell enumeration using image analysis

Image analysis was conducted using MATLAB software (MathWorks). Nuclear signals from whole-slide images of Hoechst 33342-stained specimens were extracted according to a previously published method [32]. We extracted areas with signals of Alexa Fluor 488 and Alexa Fluor 594 within tumor tissues using an auto-thresholding method [33] (Supplementary Fig. 2), and counted the number of nuclei in Alexa Fluor 488-positive and Alexa Fluor 594-positive areas to identify CD8⁺ cells and KRT7⁺ cells, respectively. The whole tumor was defined as the area within the tumor border lines drawn by the pathologist (Y.M.) on H&E images (Fig. 1b). Great care was taken not to include non-neoplastic epithelial cells, including duct cells, acinar cells, and islet cells, in the tumor areas. Using a previously established tiling method [34], regions of interest (ROIs; one ROI \approx 1mm²) were automatically defined to cover the whole-tumor areas for each case. This tiling method simultaneously defined the tumor margin regions (i.e., ROIs that were intersected by the tumor border line) and the tumor center regions (Fig. 1b). Necrotic areas, duodenal mucosa, or out-of-focus areas were manually excluded from the evaluation area. Nontissue areas, such as acellular duct lumina, were excluded using imaging techniques. Consequently, to obtain CD8⁺ cell data for 214 pancreatic adenocarcinoma cases, we analyzed 27,273 ROIs covering the whole-tumor areas (on average, 127 ROIs per case): 12,408 were located in the tumor margin, and 14,865 were located in the tumor center. On the basis of the tiling method, the tumor margin region was automatically subdivided into the inner or outer tumor margin by the tumor border line (Fig. 1b). The size of the outer tumor margin (median, 14.4 mm²; interquartile range, 6.2–12.8 mm²) was larger than that of the inner tumor margin (median, 9.7 mm²; interquartile range, 9.0–18.2 mm²). The area ratios of the outer tumor margin to the inner tumor margin showed a normal distribution among the 214 cases with logarithmic transformation ($P = 0.26$, by the Kolmogorov–Smirnov test). A second pathologist (A.U.) reviewed the KRT7-stained images in correlation with H&E

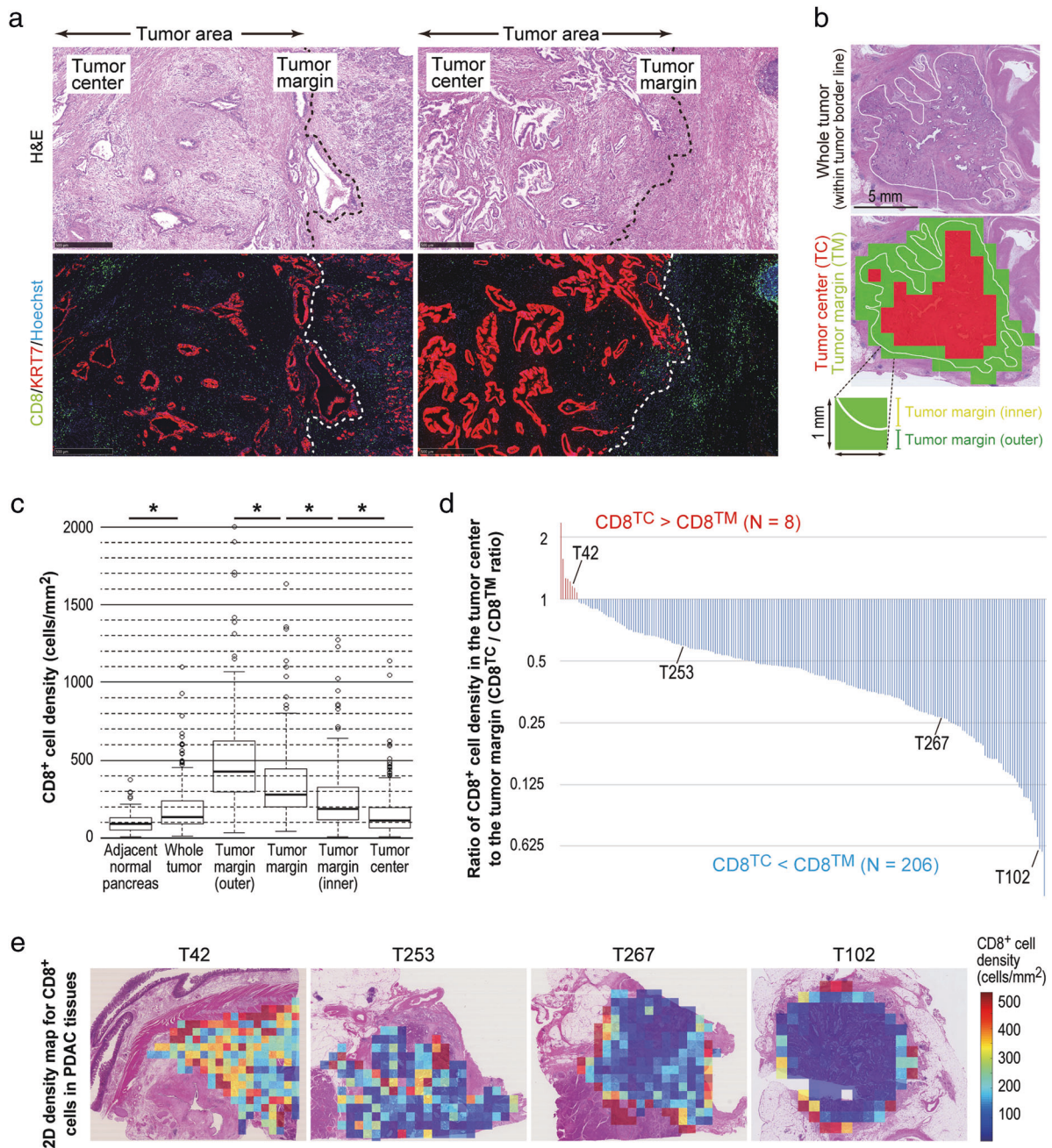


Fig. 1 Few CD8⁺ cell infiltrates were usually evident in the tumor center of pancreatic ductal adenocarcinoma. H&E and fluorescent images of pancreatic ductal adenocarcinomas with (right) or without (left) restricted infiltration of CD8⁺ T cells in the tumor center compared to the tumor margin (a). Tumor border lines annotated on a H&E image define the whole tumor (b). Regions of interests that are intersected by the tumor border line are assigned to the tumor margin. The tumor margin area was subdivided into the inner or outer tumor margin by the tumor border line. Box plots of CD8⁺ cell densities in

distinct regions within pancreatic carcinoma tissues (c). Asterisks indicate statistical significance ($P < 10^{-8}$ by the paired t test). Whiskers extend to a maximum of 1.5 times the interquartile range (boxes). A bar graph shows the ratio of CD8⁺ cell density in the tumor center to that in the tumor margin in 214 pancreatic ductal adenocarcinomas (d). Representative two-dimensional maps for CD8⁺ cell density visualizes a wide range of intratumoral heterogeneity, with a trend toward lower CD8⁺ cell density associated with inner tumoral areas (e)

images and confirmed that there were almost no non-neoplastic KRT7⁺ cells in the tumor center regions and only a small number of non-neoplastic KRT7⁺ cells in the inner tumor margin. We also selected areas of non-neoplastic

pancreatic parenchyma with minimal pathologic changes in 88 whole-tissue sections of pancreatic ductal adenocarcinomas to measure CD8⁺ cell density in adjacent normal-looking pancreas. To validate the computational data on CD8

⁺ cell density, chromogenic immunostaining for CD8 were conducted using serial sections, in which CD8⁺ cells were counted by eye by the pathologist (Y.M.) for 182 ROIs, and we confirmed a reasonable replicability of CD8⁺ cell counts (Spearman correlation coefficient, 0.98).

Outcomes

Study physicians reviewed the patients' medical records and determined the causes of death in deceased cases. In total 6 of the 214 members of the study population were excluded for survival analysis: 5 died before hospital discharge within 30 days after surgery, and one patient had a synchronous advanced intraductal papillary mucinous neoplasm. In total, 208 patients with pancreatic ductal adenocarcinoma were included in the survival analysis. The final follow-up data were collected in September 2018 with a median follow-up time of 27.0 months (range, 1.8–265.4 months).

Statistical analysis

Our primary hypothesis testing was the assessment of the associations of CD8⁺ cell densities in the whole tumor, in the tumor center, and in the tumor margin (as quartile predictor variables) with pancreatic cancer-specific survival. Deaths from causes other than pancreatic cancer were censored in the log-rank trend test and in the Cox proportional hazards regression analyses. To control for potential confounders, we conducted multivariable Cox regression analyses. Because age; sex; anatomic location; and expressions of TP53, SMAD4, and CD274 (PD-L1) were not significantly associated with pancreatic cancer-specific survival in the univariable Cox regression analysis ($P > 0.13$), we did not include these variables in the final multivariable models. The final multivariable models included CD8⁺ cell density (quartiles), year of diagnosis (continuous), tumor differentiation (grade 3 vs grade 1/2), lymphatic invasion (moderate/marked vs absent/slight), venous invasion (moderate/marked vs absent/slight), neural invasion (moderate/marked vs absent/slight), tumor stroma (scirrhous vs nonscirrhous), the extent of tertiary lymphoid structures (extensive vs minimal/absent), residual tumor status (R1 vs R0), and UICC stage (stage III/IV vs stage II vs stage I). P_{trend} value was calculated across the ordinal quartile categories of CD8⁺ cell density (1–4) as a continuous variable in the Cox regression model. We conducted similar survival analyses to assess the prognostic utility of the CD8⁺ cell proximity to tumor cells. The proportionality of hazards assumption was generally satisfied ($P > 0.05$) by evaluating time-dependent variables, which were the cross-product of the CD8⁺ cell density variable and the survival time.

To compare CD8⁺ cell densities between regions, paired t tests were performed. To assess the associations of CD8⁺ cell density with categorical variables, analysis of variance assuming equal variances was performed using an adjusted two-sided α level of 0.003 ($\approx 0.05/15$) by simple Bonferroni correction for multiple hypothesis testing. Statistical analyses were conducted using EZR version 1.35 (Saitama Medical Center) [34], which is a graphic user interface for R (the R Foundation for Statistical Computing), and all P values were two-sided.

Results

CD8⁺ cell infiltration is limited within the tumor center in most patients with pancreatic ductal adenocarcinoma

We measured the CD8⁺ cell density in whole-tissue sections from 214 patients with pancreatic ductal adenocarcinoma using multiplex immunohistochemistry-based image analysis. We observed intratumoral heterogeneity in the CD8⁺ cell distribution, with a substantial difference in cell density between the tumor center and the tumor margin in pancreatic cancer tissues (Fig. 1a). The CD8⁺ cell density in the whole tumor (mean, 198.5; median, 138.3; interquartile range, 93.0–242.2 cells/mm²) was higher than that in adjacent nontumoral pancreas with minimal pathological changes (mean, 103.8; median, 93.2; interquartile range, 55.5–136.0 cells/mm²; Fig. 1c). The CD8⁺ cell density in the tumor center (mean, 166.9; median, 112.8; interquartile range, 66.0–200.2 cells/mm²) was less than half that in tumor margin (mean, 355.9; median, 289.2; interquartile range, 206.0–448.6 cells/mm²). We found significantly fewer infiltrates of CD8⁺ cells in the inner tumor margin (mean, 251.6; median, 186.7 cells/mm²) than in the outer tumor margin (mean, 505.0; median, 430.7 cells/mm²). Among the 214 patients, 206 (96%) had a lower CD8⁺ cell density in the tumor center than in the tumor margin (Fig. 1d). Two-dimensional density maps illustrate the trend toward lower CD8⁺ cell densities in the inner tumoral areas, despite a wide range of intratumoral and intertumoral heterogeneity across our pancreatic ductal adenocarcinoma cohort (Fig. 1e).

To better characterize the differences in the tumor microenvironmental factors between the tumor center and the tumor margin, we examined immunosuppressive immune cells, fibroblasts, and the expressions of immune checkpoint ligands in pancreatic adenocarcinoma tissues (Fig. 2). Compared with the tumor center, we observed relatively high numbers of the following cells in the tumor margin areas: FOXP3⁺ cells, CD163⁺ cells including macrophages, CD11b⁺ cells including neutrophils, CD274

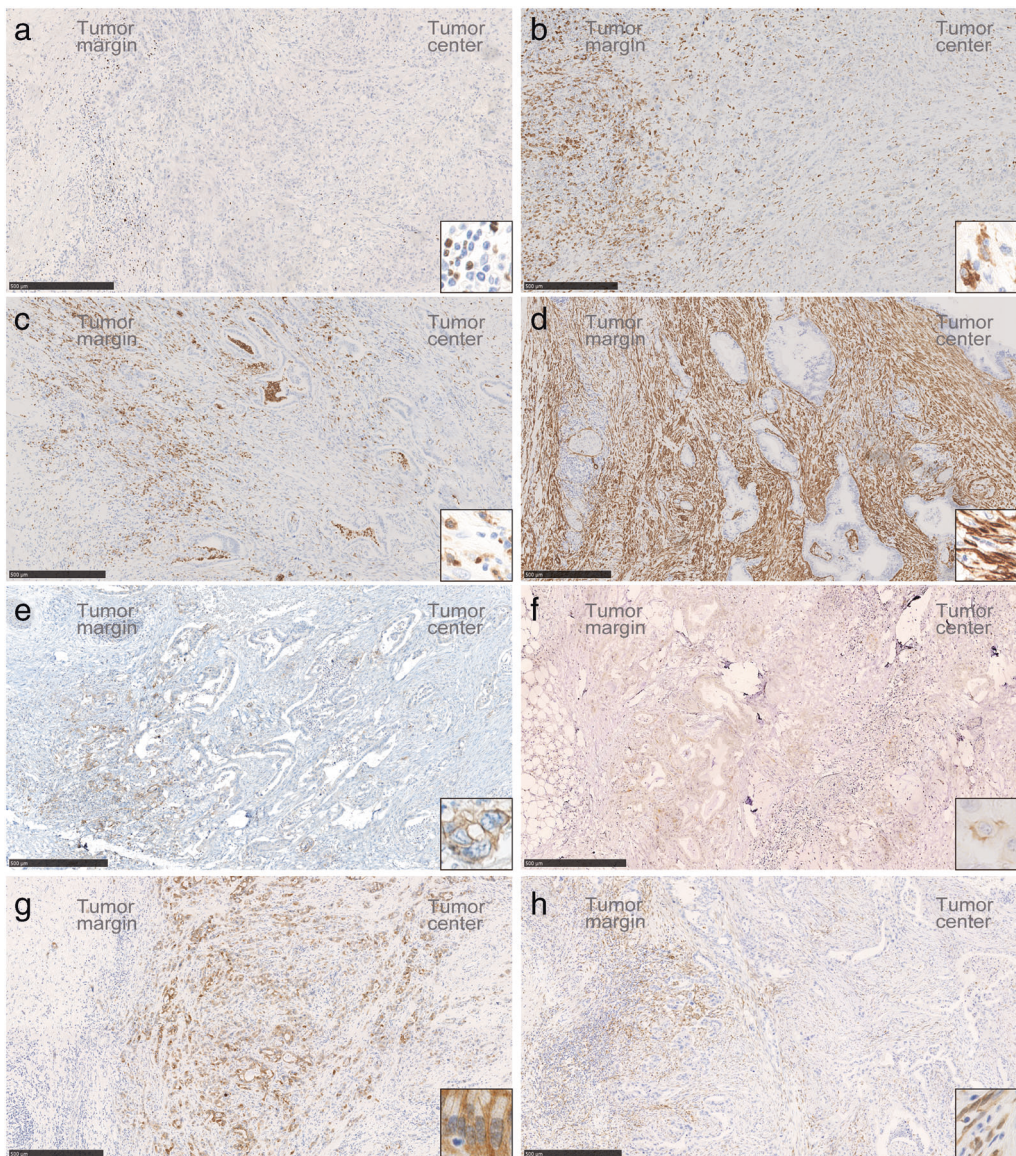


Fig. 2 Immunohistochemical analysis for regulatory T cell marker FOXP3 (a), macrophage marker CD163 (b), pan-myeloid marker ITGAM (CD11b) (c), fibroblastic marker ACTA2 (α SMA) (d), and

immune checkpoint ligands CD274 (PD-L1) (e), PDCD1LG2 (PD-L2) (f), LGALS3 (Galectin 3) (g), and LGALS9 (Galectin 9) (h) in pancreatic adenocarcinoma tissues (scale bar = 500 μ m)

(PD-L1)⁺ tumor cells and immune cells, and LGALS9 (galectin 9)⁺ stromal cells. ACTA2 (α SMA)⁺ fibroblasts were enriched both in the tumor margin and the tumor center, with no apparent differences between these two regions. LGALS3 (galectin 3) expression was present in most tumor cells, and PDCD1LG2 (PD-L2) expression was found in a small fraction of tumor cells throughout the pancreatic cancer tissues.

Clinicopathologic and prognostic significance of tumor-infiltrating CD8⁺ cells

Clinicopathologic correlations of CD8⁺ cell densities in the whole tumor, in the tumor center, and in the tumor margin

are summarized in Table 1. Although CD8⁺ cell densities showed no statistically significant correlation with the clinicopathologic factors examined ($P > 0.004$; with an adjusted α level of 0.003 for multiple hypothesis testing), there was a trend toward higher CD8⁺ cell density in the tumor margin associated with tumor CD274 (PD-L1) expression ($P = 0.037$) and with extensive tertiary lymphoid structures ($P = 0.005$). In our primary hypothesis testing, we examined the associations between CD8⁺ cell densities and pancreatic cancer-specific survival. In the log-rank trend test, CD8⁺ cell densities in the whole tumor, in the tumor center, and in the tumor margin (as quartile predictor variables) showed significant associations with better survival outcomes ($P < 0.037$; Fig. 3). Univariable

Table 1 Correlation of CD8⁺ cell density in the whole tumor, tumor center, and tumor margin with clinicopathologic features of 214 patients with pancreatic ductal adenocarcinoma

Characteristic	Total No. (N = 214)	CD8 ⁺ cell density in the whole tumor		CD8 ⁺ cell density in the tumor center		CD8 ⁺ cell density in the tumor margin	
		Mean, cells/mm ²	P*	Mean, cells/mm ²	P*	Mean, cells/mm ²	P*
Age (years)			0.61		0.49		0.66
≤65	84 (39%)	157.6		176.1		230.0	
>65	130 (61%)	169.5		161.0		238.5	
Sex			0.12		0.05		0.17
Men	132 (62%)	212.2		183.0		373.5	
Women	82 (38%)	176.4		141.0		327.7	
Year of diagnosis			0.32		0.86		0.10
Prior to 2006	103 (48%)	186.8		164.9		328.7	
2006 to 2014	111 (52%)	209.3		168.8		381.2	
Anatomic location			0.039		0.032		0.41
Head	132 (62%)	217.0		184.9		367.1	
Body/Tail	82 (38%)	168.9		138.0		339.5	
Tumor differentiation			0.73		0.36		0.09
Grade 1/2	152 (71%)	200.9		173.1		338.7	
Grade 3	62 (29%)	192.4		151.6		398.3	
Lymphatic invasion			0.58		0.56		0.70
Absent/slight	88 (41%)	180.6		159.4		363.3	
Moderate/marked	126 (59%)	214.7		172.1		350.8	
Venous invasion			0.32		0.29		0.35
Absent/slight	72 (34%)	214.4		182.8		377.2	
Moderate/marked	142 (66%)	190.4		158.8		345.2	
Neural invasion			0.56		0.81		0.12
Absent/slight	78 (36%)	207.2		163.4		388.5	
Moderate/marked	136 (64%)	193.5		168.9		337.3	
Tumor stroma			0.13		0.11		0.94
Nonscirrhous	102 (48%)	180.6		149.2		354.6	
Scirrhous	112 (52%)	214.7		183.0		357.2	
Extent of tertiary lymphoid structures			0.27		0.51		0.005
Minimal/absent	133 (62%)	188.7		161.4		320.8	
Extensive	81 (38%)	215.0		175.9		413.6	
TP53 expression			0.92		0.29		0.31
Intact	100 (47%)	199.7		179.0		338.6	
Aberrant	114 (53%)	197.4		156.3		371.1	
SMAD4 expression			0.28		0.33		0.52
Intact	84 (39%)	213.8		179.9		368.9	
Lost	130 (61%)	188.6		158.5		347.6	
CD274 (PD-L1) membrane expression			0.13		0.89		0.037
<1%	159 (75%)	189.5		166.5		338.1	
≥1%	53 (25%)	228.7		169.9		415.7	
Residual tumor status			0.46		0.32		0.69
R0	154 (72%)	193.2		160.3		360.0	
R1	60 (28%)	211.9		183.9		345.5	

Table 1 (continued)

Characteristic	Total No. (<i>N</i> = 214)	CD8 ⁺ cell density in the whole tumor		CD8 ⁺ cell density in the tumor center		CD8 ⁺ cell density in the tumor margin	
		Mean, cells/mm ²	<i>P</i> *	Mean, cells/mm ²	<i>P</i> *	Mean, cells/mm ²	<i>P</i> *
UICC stage (8 th Ed)			0.57		0.88		0.94
I	42 (20%)	215.1		176.8		371.9	
II	102 (48%)	182.1		157.8		348.7	
III	68 (32%)	211.2		174.7		358.4	
IV	2 (1%)	251.3		158.7		303.4	

*To compare mean CD8⁺ cell densities between categorical variables, analysis of variance was performed. We adjusted the two-sided α level to 0.003 ($\approx 0.05/15$) for multiple hypothesis testing

Cox proportional hazards regression analysis showed consistent results ($P_{\text{trend}} < 0.032$; Table 2). In multivariable Cox proportional hazards regression analysis, higher CD8⁺ cell density in the tumor center was significantly associated with prolonged pancreatic cancer-specific survival in a density-dependent manner ($P_{\text{trend}} = 0.002$). The multivariable hazard ratio for the highest (vs lowest) quartile of CD8⁺ cell density in the tumor center was 0.41 (95% confidence interval, 0.23–0.74; $P = 0.003$; Supplementary Table 1). In the multivariable model for CD8⁺ cell density in the tumor center, year of diagnosis, tumor differentiation, neural invasion, tumor stroma, the extent of tertiary lymphoid structure, and UICC stage, were also independent predictive factors of pancreatic cancer-specific survival. The CD8⁺ cell density in the whole tumor was also correlated significantly with pancreatic cancer mortality; however, the trend of prolonged survival with higher CD8⁺ cell density was weaker for the whole tumor than for the tumor center ($P_{\text{trend}} = 0.009$ and 0.002, respectively), likely because the relationship between CD8⁺ cell density in the tumor margin and patient survival was not significant ($P_{\text{trend}} = 0.07$).

Prognostic significance of spatial proximity of CD8⁺ cells to cancer cells in pancreatic cancer tissues

We identified 91,399,581 KRT7⁺ cells in the tumor center areas within the 214 pancreatic carcinoma tissues (on average, 42,708 cells per case) and measured the distance from each KRT7⁺ cell to the nearest CD8⁺ cell for all the KRT7⁺ cells identified (Fig. 4a). The CD8⁺ cell density in the tumor center correlated inversely with the median distance from KRT7⁺ cells to the nearest CD8⁺ cells (range, 19.9–520.1 μm ; median, 101.8) (Spearman correlation coefficient, -0.89 ; Fig. 4b). To explore the prognostic significance of CD8⁺ cell proximity to carcinoma cells, we extracted CD8⁺ cells adjacent to tumor cells (e.g., 20 μm , Fig. 4c) to measure the density of CD8⁺ cells in a given distance (10, 20, 30, 40, 50, 100, or 200 μm) from tumor

cells within the tumor center. We performed univariable Cox regression analysis and did not observe any significant association of the densities of CD8⁺ cells located within 10, 20, 30, 40, 50, or 100 μm from tumor cells with pancreatic cancer-specific survival ($P_{\text{trend}} > 0.23$; Fig. 4d). Furthermore, we calculated the distances from KRT7⁺ cells to the nearest CD8⁺ cells in the inner tumor margin. There was a strong inverse correlation between CD8⁺ cell density and the KRT7⁺ cell–CD8⁺ cell distances (range, 23.2–431.4 μm ; median, 81.2 μm) (Spearman correlation coefficient, -0.85 ; Supplementary Fig. 3A). We observed no significant prognostic association of the densities of CD8⁺ cells proximate to KRT7⁺ cells within the inner tumor margin (Supplementary Fig. 3B).

Discussion

Utilizing computational image analysis on whole-tissue sections of human pancreatic ductal adenocarcinomas, substantial intratumoral heterogeneity in terms of CD8⁺ cell density was demonstrated: there was a significant difference between the tumor center and the tumor margin, suggesting distinct immunologic milieu between these two regions. At the tumor margin of pancreatic cancer, we found a link between higher CD8⁺ cell densities and high levels of tumor CD274 (PD-L1) expression, which supports the hypothesis that CD274 is strongly upregulated by interferon gamma, a cytokine mainly produced by activated cytotoxic T lymphocytes in the tumor microenvironment [35]. Evidence indicates that nearly all pancreatic adenocarcinomas harbor tumor-specific neoantigens, several of which are linked to long-term patient survival [36–38]. In the current cohort, the abundance of CD8⁺ cell infiltrates at the tumor margin correlated with extensive tertiary lymphoid structures. These lines of evidence, together with our findings, suggest that the adaptive arm of the host immune system is involved in the elicitation of cytotoxic T cell infiltrates at

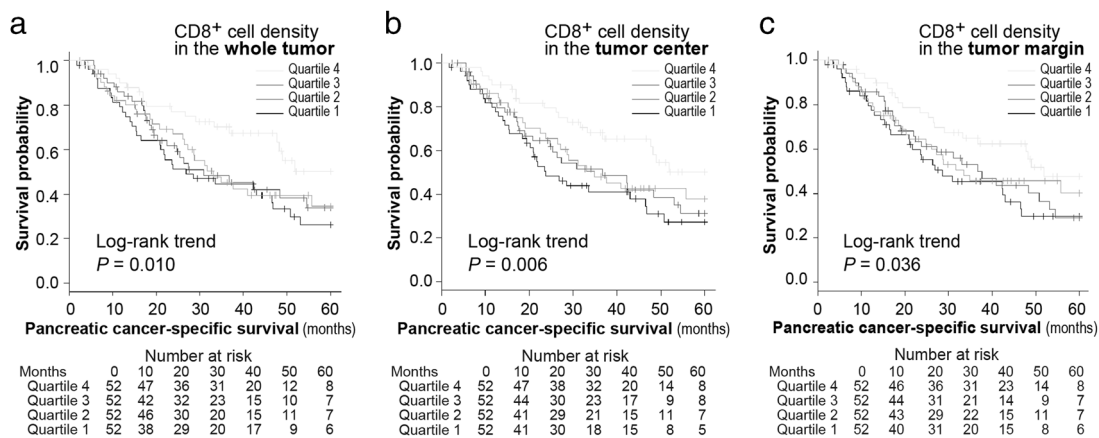


Fig. 3 Kaplan–Meier curves for pancreatic cancer-specific survival according to quartile categories of CD8⁺ cell density in the whole tumor (a), the tumor center (b), and the tumor margin (c). P values were calculated by the log-rank trend test. Tables show the number of patients who remained alive and at risk of death at each time point

Table 2 Cox proportional hazards regression analysis on the association of CD8⁺ cell density in the tumor center, tumor margin, and the whole tumor with pancreatic cancer-specific survival

	CD8 ⁺ cell density (N = 208)				P _{trend} [†]
	Quartile 1	Quartile 2	Quartile 3	Quartile 4	
Model for CD8⁺ cell density in the whole tumor					
No. of patients	52	52	52	52	
No. of deaths	32	27	28	19	
Univariable HR (95% CI)	1 (reference)	0.74 (0.45–1.24)	0.78 (0.47–1.30)	0.45 (0.26–0.79)	0.014
Multivariable HR* (95% CI)	1 (reference)	0.63 (0.37–1.08)	0.74 (0.43–1.27)	0.41 (0.22–0.73)	0.009
Model for CD8⁺ cell density in the tumor center					
No. of patients	52	52	52	52	
No. of deaths	32	28	26	20	
Univariable HR (95% CI)	1 (reference)	0.83 (0.50–1.37)	0.72 (0.43–1.21)	0.46 (0.26–0.81)	0.006
Multivariable HR* (95% CI)	1 (reference)	0.81 (0.48–1.36)	0.65 (0.38–1.12)	0.41 (0.23–0.74)	0.002
Model for CD8⁺ cell density in the tumor margin					
No. of patients	52	52	52	52	
No. of deaths	29	29	27	21	
Univariable HR (95% CI)	1 (reference)	0.93 (0.56–1.56)	0.86 (0.51–1.46)	0.55 (0.31–0.96)	0.031
Multivariable HR* (95% CI)	1 (reference)	0.70 (0.40–1.21)	0.81 (0.47–1.40)	0.52 (0.28–0.95)	0.07

CI confidence interval, HR hazard ratio

* Variables with a P value < 0.05 in the univariable Cox regression analysis were included in each multivariable model. The final multivariable models included CD8⁺ cell density variable (quartile), year of diagnosis (continuous), tumor differentiation (Grade 1/2 and Grade 3), lymphatic invasion (absent/slight and moderate/marked), venous invasion (absent/slight and moderate/marked), neural invasion (absent/slight and moderate/ marked), tumor stroma (nonscirrhous and scirrhous), the extent of tertiary lymphoid structures (minimal/absent and extensive), residual tumor status (R0 and R1), and UICC stage (stage I, stage II, and stage III/IV). Results for all the variables in the final model for CD8⁺ cell density in the tumor center are shown in Supplementary Table 1

[†] The P_{trend} value was calculated across the ordinal quartile categories of CD8⁺ cell density (1–4) as a continuous variable in the Cox regression model

the invasive front of pancreatic ductal adenocarcinoma. Moreover, findings from the current study and previous translational research have indicated limited CD8⁺ cell infiltration in the tumor center of most pancreatic carcinomas [39, 40], likely underscoring the immunosuppressive nature of the pancreatic cancer microenvironment.

A growing body of evidence indicates that stroma-modifying treatments targeting factors that functionally and mechanically suppress T cell infiltrates lead to the increase of local cytotoxic T cell infiltration, and thereby synergize the programmed cell death 1 (PDCD1, PD1)-pathway blockade agents or conventional cytotoxic chemotherapies [15, 41–45].

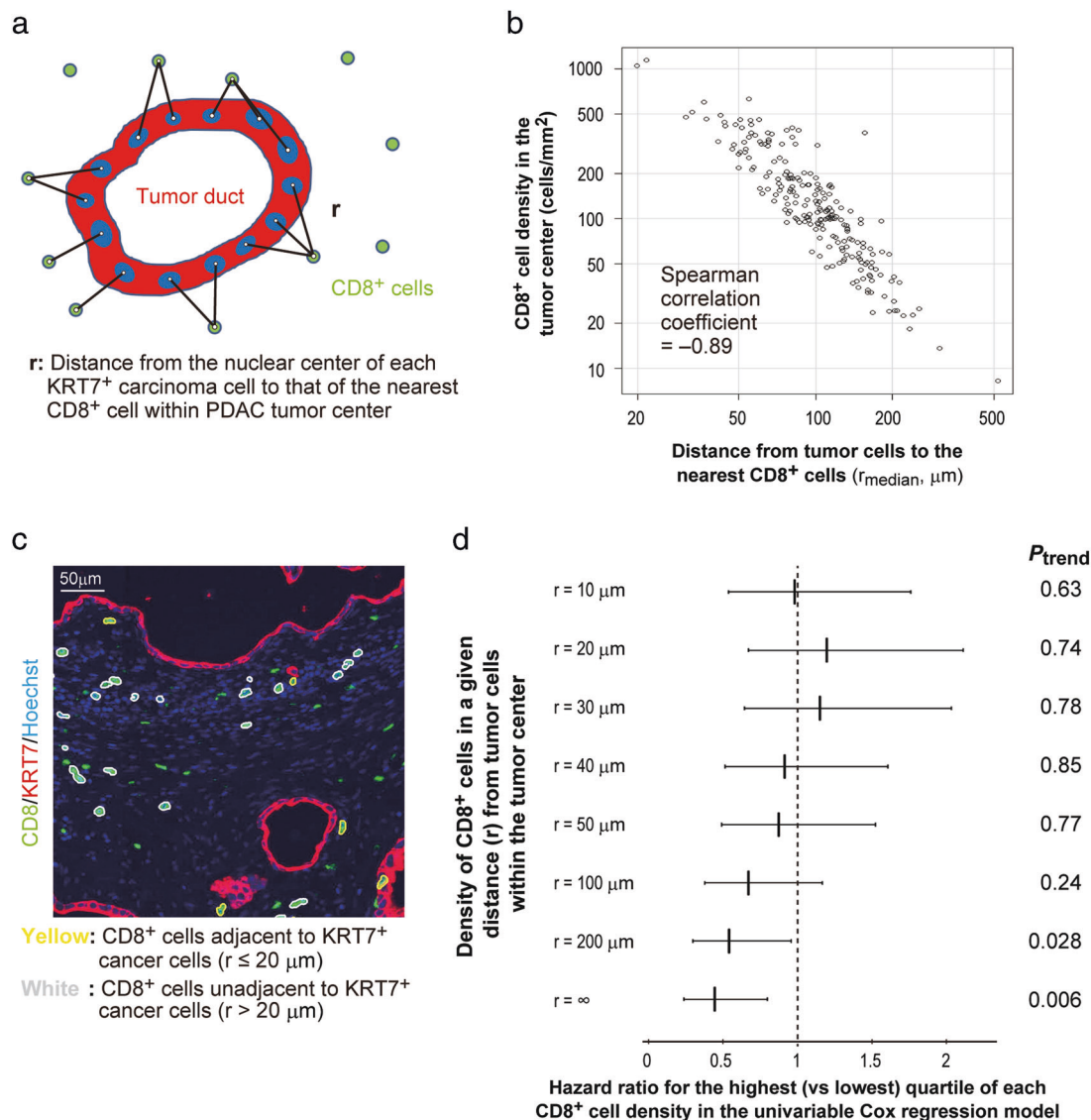


Fig. 4 Prognostic significance of the spatial proximity of CD8⁺ cells to cancer cells in pancreatic ductal adenocarcinoma. The distance between the nuclear centers of a KRT7⁺ tumor cell and its nearest CD8⁺ cell was calculated for each KRT7⁺ cell identified within the tumor center of pancreatic cancer (**a**). A scatter plot shows a strong inverse correlation of the mean distance from tumor cells to the nearest CD8⁺ cells with CD8⁺ cell density (**b**). CD8⁺ cells adjacent (e.g., $r \leq 20 \mu\text{m}$) or not adjacent (e.g., $r > 20 \mu\text{m}$) to tumor cells were extracted

from fluorescent images (**c**) and were assessed for the prognostic association with pancreatic cancer-specific survival (**d**). Hazard ratios with 95% confidence intervals for the highest (vs lowest) quartile of the densities of CD8⁺ cells within various distances from tumor cells are explored. P_{trend} values were calculated across the ordinal quartile categories of CD8⁺ cell density (1–4) as a continuous variable in the Cox regression models

Taken together, CD8⁺ cell density and intratumoral location data may constitute a promising biomarker to measure the magnitude of the anti-tumor T cell response and in situ immunosuppressive activity in the tumor immune microenvironment of pancreatic cancer.

Previous studies have shown that regulatory T cells, macrophages, myeloid-derived suppressor cells, fibroblasts, and immune checkpoint molecules suppress anti-tumor immunity in the tumor microenvironment of pancreatic cancer [11, 46]. In our analyses, FOXP3⁺ cells, CD163⁺ immune cells, ITGAM (CD11b⁺) cells, and the expressions

of CD274 (PD-L1) and LGALS9 were enriched in the tumor margin areas, rather than in the tumor center, suggesting that these factors may contribute to attenuation of the T-cell reaction at the tumor margin. In contrast, abundant ACTA2⁺ (αSMA) fibroblasts and tumor LGALS3 expressions were evident even in the tumor center regions, where CD8⁺ cell infiltrates were severely limited. Evidence indicates that pancreatic cancer desmoplasia acts as a physical barrier to immune cell infiltration and also functionally inhibits T-cell activity [43, 47, 48]. Emerging evidence attests to the importance of

heterogeneous populations of fibroblasts in the regulation of the immune contexture of pancreatic cancer stroma [10, 49]. Although our exploratory analyses using ACTA2 as a fibroblastic marker did not find any significant differences between the tumor margin and the tumor center, further studies to characterize heterogeneous components of pancreatic fibrous stroma are warranted to improve understanding of CD8⁺ cell heterogeneity within pancreatic adenocarcinoma tissues.

The current quantitative study found a significant association between intense CD8⁺ cell infiltration in the whole tumor and favorable patient survival. This finding is generally compatible with those of previous tissue microarray-based and/or semi-quantitative studies that have shown significant or borderline associations [21, 36, 50–53]. Our study additionally indicated that the prognostic association of CD8⁺ cell density with pancreatic cancer-specific mortality is significant for the tumor center, but is not statistically significant for the tumor margin. This fact indicates that the prognostic validity of CD8⁺ cell density data may depend on the tumor region in which the density is assessed. The colorectal cancer Immunoscore, which is a combination of the T cell density data at both the tumor center and the tumor margin, has proven a robust prognostic indicator [54], although analogous standardized scoring strategies for a number of other cancer types have not yet been established [55]. To accelerate the implementation of Immunoscore into routine tumor staging, further investigations are needed on how intratumor regions across various types of malignancies may modify the prognostic association of tumor-infiltrating T cells with clinical outcomes.

There was no significant correlation of the density of CD8⁺ cells proximate to cancer cells with pancreatic cancer-specific survival. In a recent study, Carstens et al. analyzed tissue microarrays from 96 patients with pancreatic ductal adenocarcinoma; however, their univariate survival analysis produced conflicting results to ours in terms of the prognostic association of CD8⁺ cell proximity to tumor cells [21]. This inconsistency likely arose as a result of differences in study designs, methods, and populations. For example, when Carstens et al. measured T-cell proximity to carcinoma cells, they utilized Ripley's L-function under the theoretical assumption that each tumor cell is isolated; however, most pancreatic adenocarcinoma cells are not isolated, but form ductular structures, as confirmed by histology [56, 57]. Of note, the L-function variable was normalized by CD8⁺ cell density, which itself was a significant prognostic factor; this procedure could potentially alter the prognostic associations. A previous study has attested to the importance of CD8⁺ cell proximity to CD274 (PD-L1)-expressing tumor cells in oral squamous cell carcinoma [58]. It is possible that the impact of CD8⁺ cell proximity to tumor cells varies for different tumor cell

subpopulations. Consequently, comprehensive spatial analyses using multiplex immunohistochemistry or other multiplex imaging techniques [59, 60] are warranted to increase our understanding of intercellular relationships between heterogeneous subpopulations of immune cells, stromal cells, and tumor cells within the tumor microenvironment of human pancreatic cancer.

One limitation in the current study is the absence of a standardized assessment of intratumoral T cell heterogeneity in tumor tissues. Nonetheless, we were able to obtain exhaustive positional information on CD8⁺ cells and carcinoma cells within whole-tissue sections of pancreatic carcinoma tissues utilizing a multiplex immunostaining system. This system allowed us to comprehensively compute CD8⁺ cell density in different regions and to measure CD8⁺ cell–tumor cell distances. Manual validation analyses using serial sections showed a reasonable reproducibility of the automated CD8⁺-cell counts in tumor tissues. Another limitation is the use of KRT7 to define carcinoma cells in the measurement of CD8⁺ cell–tumor cell distances. We observed almost no non-neoplastic KRT7⁺ cells in the tumor center regions, and only a small number of non-neoplastic KRT7⁺ cells within tumor areas of the inner margin. It is possible that the statistical power of our analyses on the distances for the latter tumor regions could be weakened by contaminating KRT7⁺ cells. Nonetheless, we obtained similar results for both regions in terms of the prognostic values of the density of CD8⁺ cells proximate to KRT7⁺ cells.

The major strengths of the current study include the automated nature and comprehensiveness of our computational analysis, which provided highly replicable data on CD8⁺ cells in pancreatic ductal adenocarcinomas. Another strength is the use of a reasonably large sample size with well-annotated clinical and pathological information, such as the tumor expression status of TP53 or SMAD4 and immune-related characteristics, including tertiary lymphoid structures and CD274 (PD-L1) expression, which enabled us to conduct a rigorous assessment of the prognostic significance of tumor-infiltrating CD8⁺ cells in pancreatic cancer tissues, adjusting for potential confounders.

In conclusion, our population-based data have revealed that pancreatic cancer is characterized by a considerably limited infiltration of CD8⁺ cells within the tumor center and that the trend of prolonged patient survival in those with higher CD8⁺ cell densities is highly significant for the tumor center, suggesting a major role of pro-tumorigenic effect of the immunosuppressive milieu of the pancreatic cancer microenvironment. Upon validation, spatial computational analysis of tumor-infiltrating CD8⁺ cells may refine their value for predicting outcomes for patients with pancreatic ductal adenocarcinoma and likely enrich our understanding of intratumoral heterogeneity in human pancreatic cancer.

Acknowledgements We are grateful to the Fourth Laboratory of the Department of Pathology in Keio University School of Medicine for assistance with tissue processing and staining.

Financial support This work was supported by KAKENHI (Grant number 18K15094 to YM) from the Japan Society for the Promotion of Science, and Keio University Academic Development Funds for Individual Research from Keio University (to YM).

Compliance with ethical standards

Conflict of interest The authors declare that they have no conflict of interest.

Publisher's note: Springer Nature remains neutral with regard to jurisdictional claims in published maps and institutional affiliations.

References

- Chen Daniel S, Mellman I. Oncology meets immunology: the cancer-immunity cycle. *Immunity*. 2013;39:1–10.
- Seo YD, Pillarisetty VG. T-cell programming in pancreatic adenocarcinoma: a review. *Cancer Gene Ther*. 2017;24:106–13.
- Vonderheide RH. The immune revolution: a case for priming, not checkpoint. *Cancer Cell*. 2018;33:563–9.
- Foucher ED, Ghigo C, Chouaib S, Galon J, Iovanna J, Olive D. Pancreatic ductal adenocarcinoma: a strong imbalance of good and bad immunological cops in the tumor microenvironment. *Front Immunol*. 2018;9:1044.
- Hiraoka N, Ino Y, Yamazaki-Itoh R, Kanai Y, Kosuge T, Shimada K. Intratumoral tertiary lymphoid organ is a favourable prognosticator in patients with pancreatic cancer. *Br J Cancer*. 2015;112:1782–90.
- Sautes-Fridman C, Lawand M, Giraldo NA, Kaplon H, Germain C, Fridman WH, et al. Tertiary lymphoid structures in cancers: prognostic value. *Front Immunol*. 2016;7:407.
- Lutz ER, Wu AA, Bigelow E, Sharma R, Mo G, Soares K, et al. Immunotherapy converts nonimmunogenic pancreatic tumors into immunogenic foci of immune regulation. *Cancer Immunol Res*. 2014;2:616–31.
- Karakhanova S, Ryschich E, Mosl B, Harig S, Jäger D, Schmidt J, et al. Prognostic and predictive value of immunological parameters for chemoradioimmunotherapy in patients with pancreatic adenocarcinoma. *Br J Cancer*. 2015;112:1027.
- Vennin C, Murphy KJ, Morton JP, Cox TR, Pajic M, Timpson P. Reshaping the tumor stroma for treatment of pancreatic cancer. *Gastroenterology*. 2018;154:820–38.
- Neesse A, Bauer CA, Ohlund D, Lauth M, Buchholz M, Michl P, et al. Stromal biology and therapy in pancreatic cancer: ready for clinical translation? *Gut*. 2019;68:159–71.
- Johnson BA 3rd, Yarchoan M, Lee V, Laheru DA, Jaffee EM. Strategies for increasing pancreatic tumor immunogenicity. *Clin Cancer Res*. 2017;23:1656–69.
- Bailey P, Chang DK, Nones K, Johns AL, Patch A-M, Gingras M-C, et al. Genomic analyses identify molecular subtypes of pancreatic cancer. *Nature*. 2016;531:47.
- Moffitt RA, Marayati R, Flate EL, Volmar KE, Loeza SGH, Hoadley KA, et al. Virtual microdissection identifies distinct tumor- and stroma-specific subtypes of pancreatic ductal adenocarcinoma. *Nat Genet*. 2015;47:1168.
- Collisson EA, Sadanandam A, Olson P, Gibb WJ, Truitt M, Gu S, et al. Subtypes of pancreatic ductal adenocarcinoma and their differing responses to therapy. *Nat Med*. 2011;17:500–3.
- Li J, Byrne KT, Yan F, Yamazoe T, Chen Z, Baslan T, et al. Tumor cell-intrinsic factors underlie heterogeneity of immune cell infiltration and response to immunotherapy. *Immunity*. 2018;49:178–93 e7.
- Lafaro KJ, Melstrom LG. The paradoxical web of pancreatic cancer tumor microenvironment. *Am J Pathol*. 2019;189:44–57.
- Birnbaum DJ, Bertucci F, Finetti P, Birnbaum D, Mamessier E. Molecular classification as prognostic factor and guide for treatment decision of pancreatic cancer. *Biochim Biophys Acta*. 2018;1869:248–55.
- Notta F, Hahn SA, Real FX. A genetic roadmap of pancreatic cancer: still evolving. *Gut*. 2017;66:2170–8.
- Knudsen ES, Vail P, Balaji U, Ngo H, Botros IW, Makarov V, et al. Stratification of pancreatic ductal adenocarcinoma: combinatorial genetic, stromal, and immunologic markers. *Cancer Res*. 2017;23:4429–40.
- Yachida S, Jones S, Bozic I, Antal T, Leary R, Fu B, et al. Distant metastasis occurs late during the genetic evolution of pancreatic cancer. *Nature*. 2010;467:1114–7.
- Carstens JL, Correa de Sampaio P, Yang D, Barua S, Wang H, Rao A, et al. Spatial computation of intratumoral T cells correlates with survival of patients with pancreatic cancer. *Nat Commun*. 2017;8:15095.
- Pagès F, Mlecnik B, Marliot F, Bindea G, Ou F-S, Bifulco C, et al. International validation of the consensus Immunoscore for the classification of colon cancer: a prognostic and accuracy study. *Lancet*. 2018;391:2128–39.
- Galon J, Mlecnik B, Bindea G, Angell HK, Berger A, Lagorce C, et al. Towards the introduction of the ‘Immunoscore’ in the classification of malignant tumours. *J Pathol*. 2014;232:199–209.
- Masugi Y, Nishihara R, Hamada T, Song M, da Silva A, Kosumi K, et al. Tumor PD-1/PD-L1 (PD-1) expression and the lymphocytic reaction to colorectal cancer. *Cancer Immunol Res*. 2017;5:1046–55.
- Ogino S, Nowak JA, Hamada T, Phipps AI, Peters U, Milner DA, et al. Integrative analysis of exogenous, endogenous, tumour and immune factors for precision medicine. *Gut*. 2018;67:1168–80.
- Kloppel G, Lingenhal G, von Bulow M, Kern HF. Histological and fine structural features of pancreatic ductal adenocarcinomas in relation to growth and prognosis: studies in xenografted tumours and clinico-histopathological correlation in a series of 75 cases. *Histopathology*. 1985;9:841–56.
- Japan Pancreas Society. Classification of pancreatic carcinoma, Fourth English Edition 4th English ed. Kanehara: Tokyo, 2017. 70–9 pp.
- Brierley JD, Gospodarowicz MK, Wittekind C. TNM Classification of Malignant Tumours, 8th edn. John Wiley & Sons, Ltd: Oxford, 2017.
- Rimm DL, Han G, Taube JM, Yi ES, Bridge JA, Flieder DB, et al. A prospective, multi-institutional, pathologist-based assessment of 4 immunohistochemistry assays for PD-L1 expression in non-small cell lung cancer. *JAMA Oncol*. 2017;3:1051–8.
- Qian ZR, Rubinson DA, Nowak JA, Morales-Oyarvide V, Dunne RF, Kozak MM, et al. Association of alterations in main driver genes with outcomes of patients with resected pancreatic ductal adenocarcinoma. *JAMA Oncol*. 2018;4:e173420.
- Yamazaki K, Masugi Y, Effendi K, Tsujikawa H, Hiraoka N, Kitago M, et al. Upregulated SMAD3 promotes epithelial-mesenchymal transition and predicts poor prognosis in pancreatic ductal adenocarcinoma. *Lab Invest*. 2014;94:683–91.
- Towards generalized nuclear segmentation in histological images. Proceedings of the 13th IEEE International Conference on Bioinformatics and BioEngineering; 10–13 Nov 2013.
- Otsu N. A threshold selection method from gray-level histograms. *IEEE Trans Syst Man Cyber*. 1979;9:62–6.

34. Kanda Y. Investigation of the freely available easy-to-use software 'EZR' for medical statistics. *Bone Marrow Transplant.* 2013;48:452–8.
35. Topalian SL, Drake CG, Pardoll DM. Immune checkpoint blockade: a common denominator approach to cancer therapy. *Cancer Cell.* 2015;27:450–61.
36. Balachandran VP, Luksza M, Zhao JN, Makarov V, Moral JA, Remark R, et al. Identification of unique neoantigen qualities in long-term survivors of pancreatic cancer. *Nature.* 2017;551:512–6.
37. Bailey P, Chang DK, Forget MA, Lucas FA, Alvarez HA, Haymaker C, et al. Exploiting the neoantigen landscape for immunotherapy of pancreatic ductal adenocarcinoma. *Sci Rep.* 2016;6:35848.
38. Poschke I, Faryna M, Bergmann F, Flossdorf M, Lauenstein C, Hermes J, et al. Identification of a tumor-reactive T-cell repertoire in the immune infiltrate of patients with resectable pancreatic ductal adenocarcinoma. *Oncoimmunology.* 2016;5:e1240859.
39. Ene-Obong A, Clear AJ, Watt J, Wang J, Fatah R, Riches JC, et al. Activated pancreatic stellate cells sequester CD8⁺ T cells to reduce their infiltration of the juxtatumoral compartment of pancreatic ductal adenocarcinoma. *Gastroenterology.* 2013;145:1121–32.
40. Stromnes IM, Hulbert A, Pierce RH, Greenberg PD, Hingorani SR. T-cell localization, activation, and clonal expansion in human pancreatic ductal adenocarcinoma. *Cancer Immunol Res.* 2017;5:978–91.
41. Mirlekar B, Michaud D, Searcy R, Greene K, Pylayeva-Gupta Y. IL35 hinders endogenous antitumor T-cell immunity and responsiveness to immunotherapy in pancreatic. *Cancer Cancer Immunol Res.* 2018;6:1014–24.
42. Nywening TM, Belt BA, Cullinan DR, Panni RZ, Han BJ, Sanford DE, et al. Targeting both tumour-associated CXCR2(+) neutrophils and CCR2(+) macrophages disrupts myeloid recruitment and improves chemotherapeutic responses in pancreatic ductal adenocarcinoma. *Gut.* 2018;67:1112–23.
43. Feig C, Jones JO, Kraman M, Wells RJ, Deonarine A, Chan DS, et al. Targeting CXCL12 from FAP-expressing carcinoma-associated fibroblasts synergizes with anti-PD-L1 immunotherapy in pancreatic cancer. *Proc Natl Acad Sci USA.* 2013;110:20212–7.
44. Jiang H, Hegde S, Knolhoff BL, Zhu Y, Herndon JM, Meyer MA, et al. Targeting focal adhesion kinase renders pancreatic cancers responsive to checkpoint immunotherapy. *Nat Med.* 2016;22:851–60.
45. Ozdemir BC, Pentcheva-Hoang T, Carstens JL, Zheng X, Wu CC, Simpson TR, et al. Depletion of carcinoma-associated fibroblasts and fibrosis induces immunosuppression and accelerates pancreas cancer with reduced survival. *Cancer Cell.* 2014;25:719–34.
46. Balachandran VP, Beatty GL, Dougan SK. Broadening the impact of immunotherapy to pancreatic cancer: challenges and opportunities. *Gastroenterology.* 2019;156:2056–72.
47. Cannon A, Thompson C, Hall BR, Jain M, Kumar S, Batra SK. Desmoplasia in pancreatic ductal adenocarcinoma: insight into pathological function and therapeutic potential. *Genes Cancer.* 2018;9:78–86.
48. Jiang H, Hegde S, DeNardo DG. Tumor-associated fibrosis as a regulator of tumor immunity and response to immunotherapy. *Cancer Immunol Immunother.* 2017;66:1037–48.
49. Biffi G, Oni TE, Spielman B, Hao Y, Elyada E, Park Y, et al. IL-1-induced JAK/STAT signaling is antagonized by TGF-beta to shape CAF heterogeneity in pancreatic ductal adenocarcinoma. *Cancer Discov.* 2018;9:282–301.
50. Mahajan UM, Langhoff E, Goni E, Costello E, Greenhalf W, Halloran C, et al. Immune cell and stromal signature associated with progression-free survival of patients with resected pancreatic ductal adenocarcinoma. *Gastroenterology.* 2018;155:1625–39 e2.
51. Lianyuan T, Dianrong X, Chunhui Y, Zhaolai M, Bin J. The predictive value and role of stromal tumor-infiltrating lymphocytes in pancreatic ductal adenocarcinoma (PDAC). *Cancer Biol Ther.* 2018;19:296–305.
52. Lohneis P, Sinn M, Bischoff S, Juhling A, Pelzer U, Wislocka L., et al. Cytotoxic tumour-infiltrating T lymphocytes influence outcome in resected pancreatic ductal adenocarcinoma. *Eur J of Cancer.* 2017;83:290–301.
53. Ino Y, Yamazaki-Itoh R, Shimada K, Iwasaki M, Kosuge T, Kanai Y, et al. Immune cell infiltration as an indicator of the immune microenvironment of pancreatic cancer. *Br J cancer.* 2013;108:914–23.
54. Ogino S, Giannakis M. Immunoscore for (colorectal) cancer precision medicine. *Lancet.* 2018;391:2084–6.
55. Donnem T, Kilvaer TK, Andersen S, Richardsen E, Paulsen EE, Hald SM, et al. Strategies for clinical implementation of TNM-Immunoscore in resected nonsmall-cell lung cancer. *Ann Oncol.* 2016;27:225–32.
56. Hruban RH, Gaida MM, Thompson E, Hong SM, Noe M, Brosens LAA, et al. Why is pancreatic cancer so deadly? The Pathologist's View. *J Pathol.* 2019;248:131–41.
57. Masugi Y, Yamazaki K, Hibi T, Aiura K, Kitagawa Y, Sakamoto M. Solitary cell infiltration is a novel indicator of poor prognosis and epithelial-mesenchymal transition in pancreatic cancer. *Hum Pathol.* 2010;41:1061–8.
58. Feng Z, Bethmann D, Kappler M, Ballesteros-Merino C, Eckert A, Bell RB, et al. Multiparametric immune profiling in HPV- oral squamous cell cancer. *JCI insight.* 2017;2:93652.
59. Angelo M, Bendall SC, Finck R, Hale MB, Hitzman C, Borowsky AD, et al. Multiplexed ion beam imaging of human breast tumors. *Nat Med.* 2014;20:436–42.
60. Levenson RM, Borowsky AD, Angelo M. Immunohistochemistry and mass spectrometry for highly multiplexed cellular molecular imaging. *Lab Invest.* 2015;95:397.